Skýrsla Matís

07 - 07

Mai 2007

Characterization of cod myosin aggregates using static and dynamic light scattering

Tom Brenner
Ragnar Jóhannsson
Taco Nicolai

ISSN 1670-7192

Skýrsluágrip Matís ohf
Matis Food Research, Innovation & Safety
Report Summary
ISSN: 1670-7192

Titill / Title	**Characterization of cod myosin aggregates using static and dynamic light scattering**		
Höfundar / Authors	*Tom Brenner, Ragnar Jóhannsson, Taco Nicolai*		
Skýrsla / Report no.	07-07		Maí 2007
Verknr. / project no.	1642	*Verknr. / project no.*	
Styrktaraðilar / funding:	*Matís, Rannís, AVS*		

Ágrip á íslensku:

Myosin var einangrað úr þorski með mismunandi aðferðum sem skiluðu klösum af hreinu myosini. Þessir klasar innihéldu milli 8 og 20 myosin sameindir, og voru stöðugir við kaldar aðstæður (T<20°C) og í þynntum lausnum (C<5g/L) með 0.5M KCl við pH 6.0 til 8.0. Við hærri styrk próteins geljaðist það eða féll út. Klösunin við lágan styrk var skoðuð með gleypnimælingum og ljósdreifingu. Klösunin hætti eftir langan hitunartíma í flestum tilfellum, en við ákveðnar kringumstæður hélt hún þó áfram og leiddi til útfellingar próteinsins. Kæling leiddi til frekari klösunar, sem virðist vera afturkræf m.t.t. endurhitunar.

Bygging klasanna var ákvörðuð eftir kælingu og útþynningu. Sjálflíkir klasar voru greindir, með brotvídd 2.2. Stærð klasanna jókst með hækkandi hitastigi (30-70°C), hækkandi próteinstyrk (0.4-3 g/L) og lækkandi pH (8.0-6.0). Bygging klasanna var hins vegar óháð myndunaraðstæðum.

Lykilorð á íslensku: *þorskmyosin, klösun, ljósdreifing.*

Summary in English:

Myosin was extracted from Atlantic Cod (*Gadus Morhua*) using different methods resulting in small aggregates of pure myosin. These aggregates consisted of between 8 and 20 myosin molecules and were relatively stable at low temperatures (T<20°C) in dilute (C<5g/L) solutions containing 0.5M KCl in the pH range 6.0-8.0. At higher concentrations precipitation or gelation was observed. Heat induced aggregation at low concentrations was studied using turbidimetry and light scattering. In most cases the aggregation stagnated at longer heating times, but in some cases the aggregation continued until it led to precipitation of large flocs. Cooling led to further growth of the aggregates, which was, however, reversed upon heating.

The structure of the aggregates was determined after cooling and dilution using static and dynamic light scattering. Self-similar aggregates were observed, characterized by a fractal dimension of 2.2. The size of the aggregates formed after extensive heating increased with increasing temperature (30-70°C), decreasing pH (8.0-6.0) and increasing protein concentration (0.4-3g/L), but the structure of large aggregates was independent of the conditions.

English keywords: *cod myosin, aggregation, light scattering.*

TABLE OF CONTENTS

1. INTRODUCTION

The cardinal role played by myosin in muscle protein gel formation and in binding of meat is well documented [1,2]. Muscle myosin (Myosin II), the main component of the myofibrillar proteins, is comprised of two heavy chains of about 220 kDa, and 4 light chains of about 20 kDa each[3]. Myosin's heavy chain is composed of a long α-helix tail and a globular head. The two heavy chains are woven together, to form a tail and two pear-shaped heads [4-6]. The tail is 155 nm long, with a diameter of 2 nm, while the heads have a long axis of about 20 nm and a short axis at the widest point of about 6 nm.

Pure myosin can be solubilized in salt water, but aggregates when heated, which may lead to gelation when the concentration is sufficiently high. Most research on myosin aggregation and subsequent gelation has been performed on mammalian myosin [5,7-12]. Less work has been done on aggregation of fish myosin [13-16], which is less stable than mammalian myosin [14,17-20]. Variance in myosin stability is also found between different fish species, with an apparent correlation between the thermal stability of myosin and the species habitat [20-22].

The aggregation process of myosin molecules is thought to consist of two steps [5,10-12]. In the first step oligomers are formed by association of the heads, possibly through disulfide bridge formation. Tazawa et al. [16] found for fish myosin that oligomerisation can also occur by association of the so-called neck regions between the heads and the tails. Electron microscopy images of the oligomers showed star-like clusters with the heads assembled in the centre and the tails radiating out [5,16,23-25]. During the second step of the process the oligomers aggregate to form larger clusters, possibly involving association of the tails. Very little is known about the structure of these larger aggregates. Eventually, the growth of the clusters may lead to the formation of a system spanning network. Cooling of the system was reported to have an influence both on the clusters and the gel formed by whole myosin [15] or the rod fraction of myosin [26].

The objective of the work presented here was to investigate the aggregation of myosin using static and dynamic light scattering. These techniques have so far rarely been used to study myosin aggregation, but were found to be useful for the characterization of heat induced aggregation of other important food proteins such as ovalbumin and β-lactoglobulin (β-lg) [27]. The advantage of scattering techniques

compared to electron microscopy is that they require no sample treatment and that they can be used in-situ during the aggregation process.

The myosin used for this study was isolated from cod. Cod myosin is highly unstable and spontaneously aggregates in solution even at low temperatures. We will show that myosin solutions obtained using the isolation method recommended by Kristinsson [28], which consisted of a slightly modified version of a method reported initially by Martone et al. [29], contained oligomers of myosin and in addition larger aggregates. A simplified isolation method was also used that led to smaller oligomers and fewer large aggregates at the expense of a slightly lower purity. Further heat induced aggregation of the oligomers was studied at different protein concentrations (0.4-3g/L), heating temperatures (30-70°C) and pH (6.0-8.0). The ionic strength was kept constant at 0.5M KCl. The structure of the aggregates was determined after cooling and dilution.

2. MATERIAL & METHODS

Sample Preparation

White muscle (free of connective tissue) of cod fillets was treated to obtain myosin, following the method proposed by Martone et al. [29] as modified by Kristinsson [28] (method 1), as well as a shorter method described below (method 2). The fish was kept on ice post mortem (between 1 and 4 days) before use and was thus in the state of rigor mortis or immediate post rigor mortis.

Method 1. Chopped muscle was homogenised in solvent A (0.1 M KCl, 1 mM phenylmethylsulfonylfluoride, 0.02% NaN_3 and 0.02 M Tris-HCl buffer, pH 7.5) and kept for 60 minutes on ice, before centrifugation at 1000 g for 10 minutes. The pellet was dispersed in solvent B (0.45 M KCl, 5 mM β-mercaptoethanol (MCE), 1mM ethylene glycol-bis (β-aminoethyl ether) N,N,N',N'-tetraacetic acid, 0.2 M Mg^{2+} and 0.02 M TRIS-maleate buffer, pH 6.8), before adding either ATP or $K_2P_4O_7$ to a final concentration of 10 mM. The dispersion was kept in solvent B for 90 min. during which

myosin is extracted into the solution, while actin remains insoluble. After centrifugation the supernatant containing the myosin (supernatant 2) was diluted by a factor 25 in 1 mM $NaHCO_3$, which led to precipitation of the myosin. The myosin was recovered by centrifugation at 10,000 g for 10 minutes and the pellet was dispersed in solution C (0.5 M KCl, 5 mM MCE and 0.02 M TRIS-HCl buffer, pH 7.5) using a Potter-Elvehjem tissue grinder. Myosin was precipitated again by dilution (3x) in 1mM $NaHCO_3$ with 10 mM Mg^{2+} and the myosin was recovered by centrifugation after keeping the solution over night in the cold. Myosin solutions were prepared by dissolving the pellet in 0.5M KCl.

The purity of the myosin as determined by SDS-PAGE was very high. The only impurity was a very small quantity (<3%) of actin. No difference in the myosin purity was observed when using $K_2P_4O_7$ instead of ATP, as well as when leaving MCE out of all the extraction steps. ATP has the disadvantage of absorbing light at a wavelength of 280nm, which perturbs the determination of the protein concentration using absorbance.

Unfortunately, solutions of myosin prepared using method 1 were difficult to filter through 0.45µm pore size filters, and obviously contained very large aggregates. Attempts to prepare solutions with higher concentrations (>5g/L) showed the presence of large insoluble flocs. It was suspected that large aggregates were formed during the myosin precipitation step. Therefore we modified the extraction procedure as follows in order to avoid precipitation of the myosin (method 2).

Method 2. Method 1 was followed to obtain supernatant 2. One washing step of pellet 1 with 0.05 M KCl was added (prior to the dispersion in solvent B). MCE was not added, and $K_2P_4O_7$ was used instead of ATP. Instead of precipitating the myosin, supernatant 2 was extensively dialyzed against 0.5 M KCl buffered at the pH of choice (6.5-8) at 4°C. NaN_3 was added (0.02%) to avoid protein degradation. Care was taken to perform all extraction steps at a temperature not exceeding 5°C. Solutions at pH 6.0 aggregated relatively rapidly even at 4°C. Therefore solutions at pH 6.0 were made by adjusting the pH of solutions dialysed against pH 7.

The purity of the myosin obtained by method 2 was close to that obtained by method 1 with only a small additional contamination of tropomyosin (<2%). Solutions of myosin obtained by method 2 contained fewer large aggregates, which shows that precipitation leads to irreversible aggregation of a fraction of the myosin.

The concentration of myosin in supernatant 2 was rather low (3-6 g/L). Therefore an attempt was made to concentrate myosin using reverse osmosis. Dialysis bags with myosin solutions were placed in concentrated (100 g/L) solutions of polyethylene oxide with weight average molar mass (M_w) equal to 10^5g/mol. The approximate concentration of myosin was monitored by weighing the dialysis bag before and during dialysis. The concentration increased substantially after overnight dialysis. However, the more concentrated myosin aggregated and gelled in the dialysis bags.

For light scattering experiments the myosin solutions were filtered through 0.45μm pore size filters in order to remove large aggregates and other spurious scatterers. The myosin concentration was determined using UV absorbance after filtration, as described below. Only relatively low concentrations (<5g/L) of myosin prepared by method 1 could be filtered. We observed that unfiltered solutions at concentration between 7 and 10 g/L (pH 7) gelled over the course of 2 to 8 weeks at 4°C exhibiting extensive syneresis, especially at the lowest concentrations. Similar observations were reported by Connell [17].

Determination of the myosin concentration using UV absorption

The extinction coefficient (ε) of cod myosin at 278 nm was determined as follows. The absorbance of myosin solutions was measured using a spectrophotometer (Varian). Most of the myosin was subsequently precipitated by dilution with distilled water. The small residual amount of myosin that did not precipitate was estimated by measuring the absorbance of the supernatant. The precipitated myosin was then dried in vacuum at 80°C for 4 days to remove remaining water, and subsequently weighed. The value of the extinction coefficient determined in this way was 0.75 $L.g^{-1}.cm^{-1}$. This value may be compared with the values reported by Woods et al. [30], who found the value of rabbit and lobster myosin in 0.5 M HCl to be 0.54 and 0.78 $L.g^{-1}.cm^{-1}$, respectively.

SDS-PAGE

The electrophoretic pattern of solutions was determined using pre-cast polyacrylamide 4-15% gel slabs (Bio-Rad Laboratories Inc., Herts, UK) run on an electrophoresis unit (Bio-Rad, miniprotean II Cell) with a constant current of 60 mA per gel. The gels were scanned with a GelDoc 2000 scanner (Bio-Rad Laboratories Inc., Herts, UK)) and analyzed using the software package GelCompar II, 2.01 (Applied Maths BVBA, Kortrijk, Belgium). Broad range protein standards were obtained from Bio-Rad Laboratories (Bio-Rad Laboratories Inc., Herts, UK).

Turbidity

Myosin solutions were placed in quartz cells (inner diameter = 10 mm), and the lid was sealed with parafilm to avoid evaporation. The cells were placed in a holding chamber, equipped with water jackets, and the temperature was controlled to within 0.2°C using a water bath. The turbidity at different wavelengths was measured using a spectrophotometer Varian Cary-50 Bio (Les Ullis, France).

Light Scattering

Static and dynamic light scattering measurements were made using an ALV-5000 multiple tau digital correlator (ALV-Langen, Germany) and a JDS Uniphase He-Ne laser (vertically polarized beam, wavelength 632.8 nm), model 1145P-3083. This laser was provided with the ALV goniometer system (ALV/CGS-8). The range of scattering wave vectors (q) covered in the experiment was $2.8\times10^{-3} - 2.6\times10^{-2}\,\mathrm{nm}^{-1}$. The scattering vector q is given as $q = (4\pi n_s / \lambda)\sin(\theta/2)$, where n_s is the refractive index of the sample and θ is the scattering angle. The temperature of solutions in light scattering experiments was controlled to within 0.2 °C using a thermostat water bath.

Analysis of light scattering data

The relative excess scattering of particles is related to their weight average molar mass, M_w, and their structure factor, S(q) [31,32]:

$$I_r = KCM_wS(q) \qquad 1$$

where K is a constant, C is the particle mass concentration. At infinite dilution S(q) depends on the particle size and shape and can be related to the z-average radius of gyration (R_{gz}):

$$S(q) = \left(1 + (q.R_{gz})^2 / 3\right)^{-1} \qquad qR_{gz}<1,\ C\rightarrow 0 \qquad 2$$

If one applies eqs 1 and 2 to results obtained at finite concentrations one obtains an apparent molar mass (M_a) and radius of gyration (R_{ga}). At low concentrations the effect of interactions can be described in terms of the second virial coefficient (A_2).

$$S(q) = \left(1 + 2A_2C\right)^{-1} \qquad 2A_2C<1,\ q\rightarrow 0 \qquad 3$$

M_w, R_{gz} and A_2 are obtained by extrapolation of measurements at different values of q and C. A convenient representation of the data and the extrapolations is the so-called Zimm plot in which KC/I_r is plotted as a function of data against q^2+bC, with b an arbitrary constant.

With the technique of dynamic light scattering (DLS) the autocorrelation function of the scattered light intensity fluctuations is determined [31,33]. The normalized autocorrelation function ($g_2(t)$) can be analyzed in terms of a distribution of exponential decays:

$$g_2(t) - 1 = \left[\int A(\tau) \exp\left(-\frac{t}{\tau} \right) d\tau \right]^2 \qquad 4$$

where $A(\tau)$ is the amplitude of the exponential with relaxation time τ. In dilute solutions and for $qR_{gz}<1$, the relaxation of intensity fluctuations is caused by centre of mass diffusion of the particles and τ depends on the diffusion coefficient of the particles (D):

$$\tau = (q^2 D)^{-1} \qquad R_{gz}<1,\ C \rightarrow 0 \qquad 5$$

D is related to the hydrodynamic radius, R_h, through the Stokes-Einstein relation:

$$D = kT/(6\pi\eta R_h) \qquad 6$$

with T the absolute temperature, k Boltzmann's constant and η the viscosity. For polydisperse solutions a distribution of relaxation times will be observed that corresponds to the distribution of hydrodynamic radii. Eqs 5 and 6 are only valid if $q.R_g<1$, otherwise rotation and internal dynamics may play a role in the relaxation process. For fully flexible particles $D \propto q^{-1}$ if $qR_g>>1$. Autocorrelation functions were analyzed in terms of eq.4 using the REPES [34] and CONTIN [35] routines, which gave similar results. The z-average hydrodynamic radius (R_{hz}) was obtained from the average diffusion coefficient using eq. 6. At finite concentration an apparent hydrodynamic radius (R_{ha}) was obtained in this way.

3. RESULTS

Characterization of unheated myosin solutions

Solutions of isolated myosin were characterized at 20°C using static and dynamic light scattering. Figure 1 shows an example of a Zimm plot for myosin obtained by method 2 at pH 8. From extrapolations to $q \rightarrow 0$ and $C \rightarrow 0$ the following values for the weight average molar mass, the z-average radius of gyration and the second virial

coefficient were obtained: $M_w = 6.3\times10^6$ g/mol, R_{gz} = 80 nm and $A_2 = 1.4*10^{-8}$ mol.L.g^{-2}. It appears that the isolation procedure used here did not yield solutions of individual myosin. Comparison with the values for individual myosin given in the literature [36] ($M_w=5\times10^5$ g/mol and R_g=45nm) shows that oligomers containing on average about 12 myosin molecules were formed during the isolation procedure.

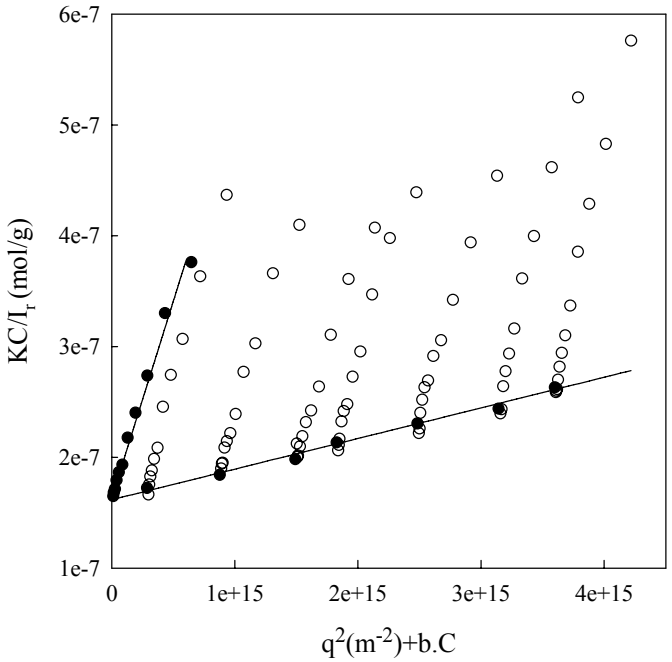

Fig.1 Zimm plot obtained for myosin isolated using method 2 in aqueous solutions at pH 7. The filled points represent extrapolations to q=0 and C=0 of the data at constant C and q, respectively. The solid lines are linear least squares fits to the extrapolated data.

Figure 2 shows the apparent molar mass of myosin solutions as a function of the concentrations for different preparations which illustrates several general trends. Oligomers with a weight average aggregation number between 8 and 20 myosin molecules were obtained in all cases. The largest oligomers were obtained with method 1. With method 2 larger oligomers were obtained if the dialysis was longer or done at higher temperatures. In the pH range between 6 and 8, generally, smaller oligomers were obtained at higher pH that grew more slowly during storage. At pH 8 the oligomers were very stable at 4°C showing a typical increase of M_w between 20-30% over a period of a month. The observed effect of the pH on the stability is in agreement with the results reported by Connell [17] who reported that cod myosin was most stable at pH 7.5-8.

In all cases a small positive second virial coefficient was observed in the range 1.4-2.5*10^{-8} mol.L.g^{-2}. The hydrodynamic radius of the oligomers was around 100 nm, while the radius of gyration was in the range 70-90 nm. These values depended little on the preparation method. We note that Kouchi et al. [15] observed a hydrodynamic radius of 95 nm for myosin isolated from white croaker, which implies that their isolation method also produced oligomers. We used for the experiments described in the following, only myosin prepared by method 2.

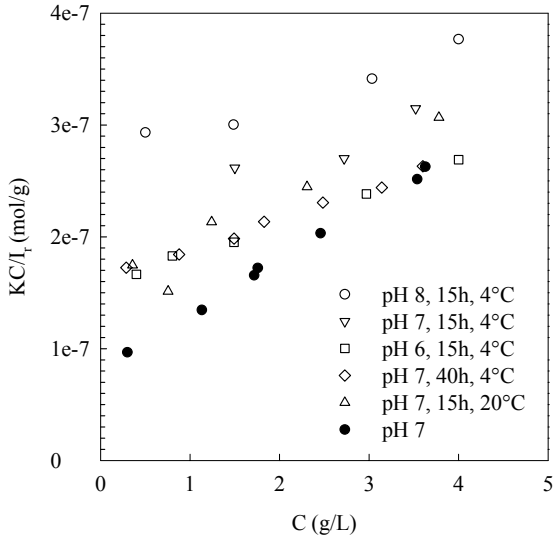

Fig.2 Comparison of the concentration dependence of KC/I_r for myosin solutions obtained in different ways. Results for myosin isolated using methods 1 and 2 are represented by filled and open symbols, respectively.

Thermally induced aggregation of myosin

Figure 3 shows the turbidity of myosin solutions with C = 5 g/L during heating at 50°C for different values of the pH. The turbidity increased sharply during the first few minutes followed by a much weaker increase. Similar observations were reported by Gill et al. [14] for cod and herring myosin at pH 6.5, but they plotted the data on a linear time scale so that the weak long time increase is not seen as clearly from their results. Gill et al. studied the effect of the salt concentration (0.6-1.4M NaCl) and the heating

temperature (35-55°C). They found that the turbidity increased faster at higher heating temperatures to reach values that increased weakly with increasing salt concentration. In the present study, we also observed a faster increase of the turbidity with increasing temperature reaching values that increased weakly with decreasing pH from pH 8 to pH 6.5. However, at pH 6.0 the increase was much stronger and at long heating times precipitation was observed. The most likely explanation for the increase of the turbidity is, of course, that the molar mass of the myosin aggregates increased.

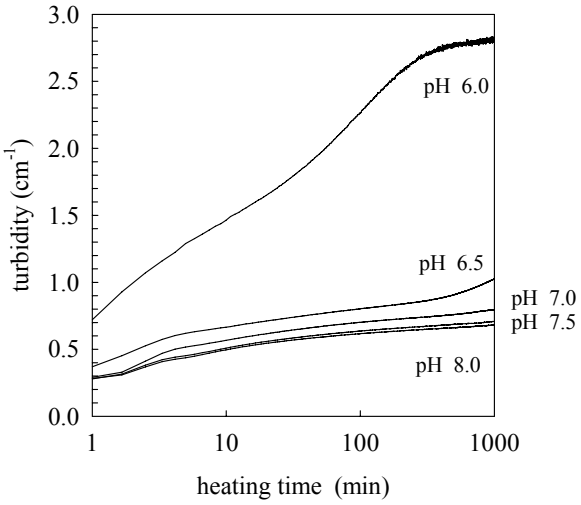

Fig.3 Dependence of the turbidity at λ=350nm on the heating time at 70°C for myosin solutions with C=5.0 g/L at different values of the pH.

We have studied the variation of the apparent molar mass, radius of gyration and hydrodynamic radius of myosin during heating using light scattering. Fig. 4a shows the evolution of M_a at 50°C for three different values of the pH with C=1.5g/L. M_a increased rapidly at first and then stagnated for pH 7 and pH 8, but it continued to increase at pH 6.0. The increase of M_a at pH 7 and 8 was modest, but at pH 6 it was important. In fact, the solutions at pH 6 became turbid after long heating times so that light scattering results are no longer reliable. The results for M_a confirm those obtained from the turbidity measurements showing a modest heat induced aggregation between pH 6.5 and 8.0 and a much more extensive aggregation at pH 6.

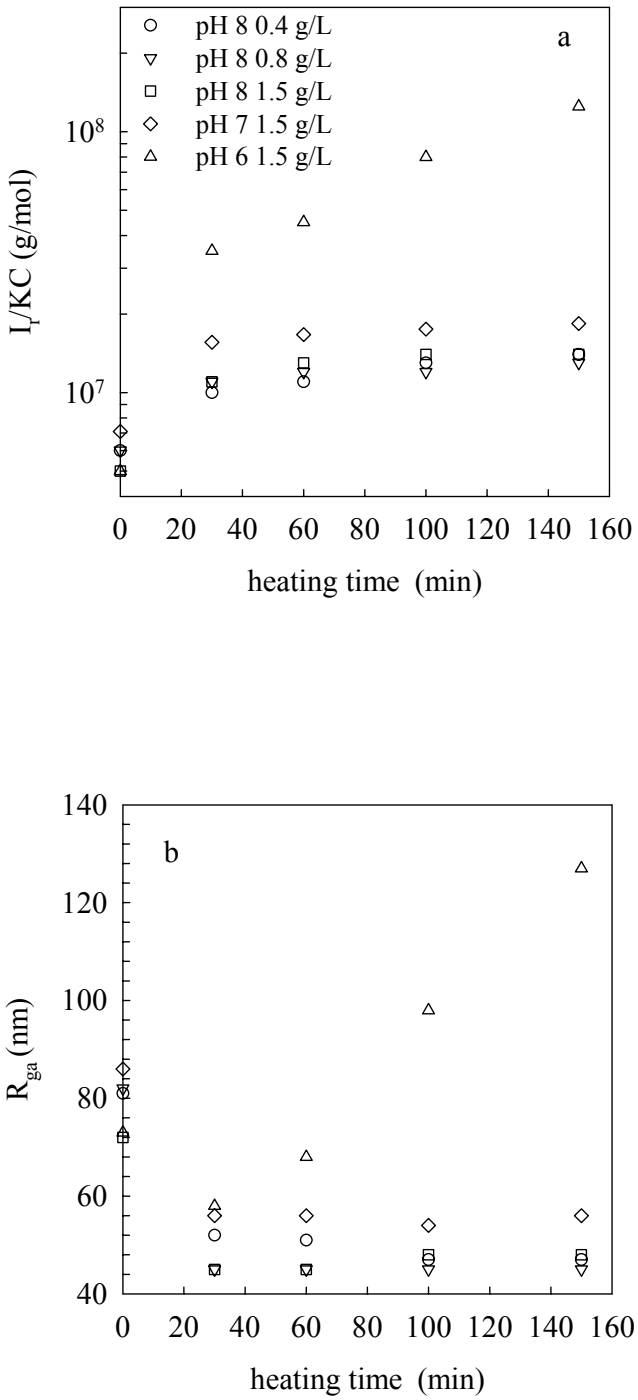

Fig.4 Dependence of KC/I_r (a) and R_{ga} (b) on the heating time at 50°C for myosin solutions at different concentrations and pH.

Surprisingly, while M_a increased, R_{ga} and R_{ha} decreased substantially. Fig. 4b shows the dependence of R_{ga} on the heating time. Similar results were found for R_h (results not shown).The effect of heating on R_{ga} and R_{ha} is thus the inverse of that on M_a. Kouchi et al. [15] noted a similar decrease of R_{ha} for myosin of white croaker when increasing the temperature from 20°C to 40°C. At pH 7 and pH 8 the radii remained constant at longer heating times, but at pH 6 the values reached a minimum and increased at longer times. It is clear that the aggregation process at pH 6 at longer heating times has a different character.

Results obtained at different concentrations (0.4, 0.8, 1.5 and 3.0g/L) and temperatures (30, 50 and 70°C) showed in all cases initially a rapid increase of M_a and a decrease of R_{ga}, although the effect was slower and less pronounced at 30°C. The subsequent slow increase of both M_a and R_{ga} was not observed within 15h at pH 8. It was observed at pH 7 at 70°C for 1.5 and 3.0g/L. At pH 6 it was observed for 1.5 and 3.0g/L both at 50°C and 70°C. In general, the rate of the second aggregation process at longer heating times increased with increasing protein concentration, increasing heating temperature and decreasing pH.

If the myosin oligomers are indeed formed by association of the heads as suggested on the basis of electron microscopy, then the initial increase of the M_a can be understood in terms of an increase of the association number. However, for star polymers the radius increases with increasing association number, albeit weakly [37], while for myosin oligomers a decrease of both R_g and R_h was observed. The origin of this phenomenon is probably the transition of the tail structure from a helix to a random coil [5,9-12,23]. As a consequence, the tails become less rigid and therefore less extended resulting in smaller values of R_g and R_h.

Effect of cooling after prolonged heating

We have seen that between pH 6.5 and 8.0 heating led initially to an increase of the molar mass and a decrease of the size of the myosin aggregates, but that at longer heating times the variation was very weak. For this reason the turbidity of heated solutions increased rapidly at first and only very slowly at longer times. Figure 5 shows

the effect of cooling and reheating on the turbidity of myosin solutions (C=5g/L) after prolonged (15 hours) heating at 50°C. Cooling to 20°C led to an increase of the turbidity at the same rate as the temperature change, which means that the molar mass of the aggregates increased. The increase was stronger with decreasing pH between 8.0 and 6.5. Interestingly, reheating to 50°C decreased the turbidity back to the same value, implying that the increase was reversible.

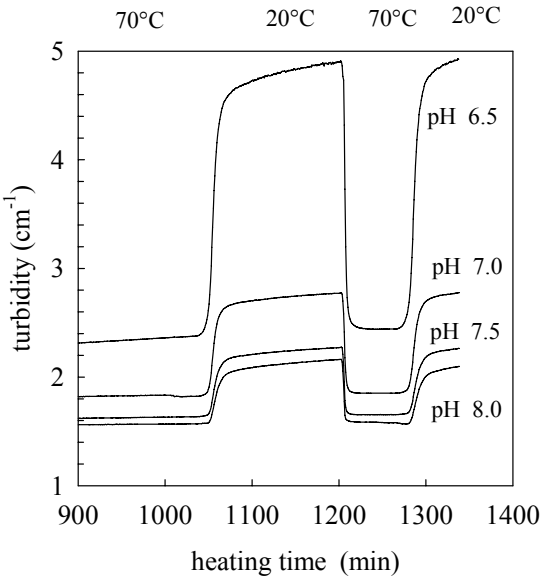

Fig.5 Effect of cooling and heating cycles on the turbidity of extensively heated myosin solutions with C=5.0 g/L at different values of the pH.

The effect of cooling to 20°C on M_a, R_{ga} and R_{ha} was determined for several myosin solutions after prolonged heating. An increase of these parameters was observed after cooling, except at pH 8 and C=0.4g/L for which no effect of cooling was observed. The effect of cooling was stronger at higher myosin concentration, at higher heating temperature, and at lower pH. It was verified for several solutions that the effect of cooling was reversible upon reheating.

Structure of myosin aggregates

The structure of myosin aggregates formed by heating was studied at 20°C using light scattering. Heated myosin solutions were cooled to 20°C and highly diluted so that the influence of interactions on the measurements could be neglected. Aggregates formed at different myosin concentrations (0.4-3g/L), different pH (6, 7 and 8) and different heating temperatures (30°C, 50°C and 70°C) were studied. Figure 6a, shows the q-dependence of I_r/KC for a number of solutions containing aggregates of different size formed by heating at 70°C at different conditions of pH and myosin concentration. M_w and R_g were derived from the initial q-dependence using eqs 1 and 2. As mentioned above, in general, the size of the aggregates increased with increasing myosin concentration, increasing heating temperature and decreasing pH.

At pH6 very large aggregates were formed that showed a power law q-dependence of KC/I_r over the whole accessible q-range:

$$\frac{I_r}{KC} \propto q^{-d_f} \qquad 7$$

A power law q-dependence of the structure factor is characteristic for self-similar structures and the exponent is equal to the so-called fractal dimension (d_f). A linear least squares fit gave d_f=2.2 for myosin aggregates, see solid line in figure 6a. Similar results were obtained for solution heated at 50°C. At 30°C only relatively small aggregates were formed at the concentration and pH conditions tested in this study (data not shown).

The formation of self-similar aggregates by proteins upon heating has been reported earlier for β-lactoglobulin[38,39], ovalbumin [40]and bovum serum albumin [41] with values for d_f close to two. It was found that the structure factor of aggregates of different size superimposed if plotted as a function of $q.R_g$. The master curve obtained by superposition of the data plotted in figure 6a is shown in figure 6b. In fact, the structure factor of myosin aggregates formed at all conditions tested superimposed on the same master curve within the experimental error.

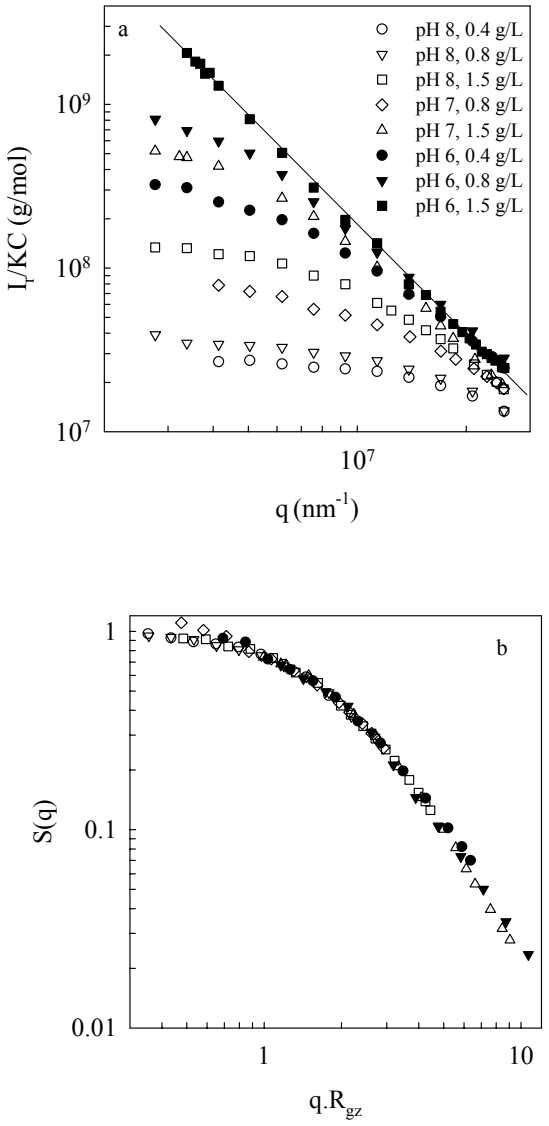

Fig.6a q-dependence of I_r/KC for highly diluted aggregate solutions obtained by extensively heating at 70°C myosin solutions at different concentrations and pH. The solid line has slope -2.2.
Fig.6b Same data as plotted in figure 6b after normalizing I_r/KC with M_w and q with R_{gz}.

Figure 7 shows M_w as a function of R_g for all samples. For self-similar aggregates a power law relationship is expected:

$$M_w = a.R_{gz}^{d_f} \qquad 8$$

where the prefactor a is determined by the local structure of the aggregates. The data plotted in figure 7 show relatively large scatter, but they are consistent with eq.8 using the same value for the fractal dimension (d_f=2.2), see solid line. Figures 6b and 7 represent the central result of this work. They show that large cod myosin aggregates formed after heating and subsequent cooling have the same self-similar structure independent of the heating temperature, the myosin concentration and the pH. The fact that the prefactor a is independent of the heating conditions within the experimental error, shows that also the local structure of the aggregates is approximately the same.

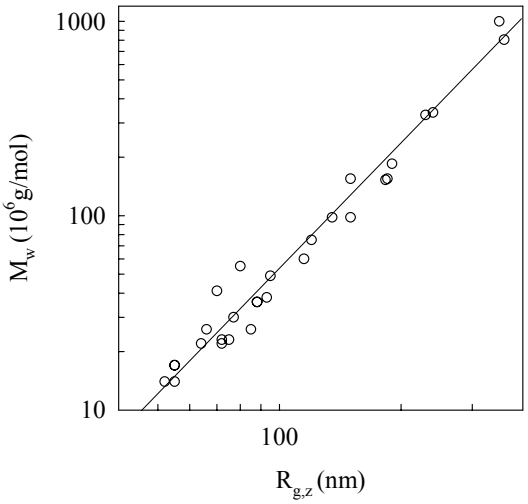

Fig.7 Dependence of the molar mass on the radius of gyration for myosin aggregates obtained at different heating temperatures, concentrations and pH. The solid line has slope 2.2.

An independent measure of the size of the aggregates is the hydrodynamic radius. Autocorrelation functions were determined for dilute solutions of myosin aggregates obtained at different conditions. The analysis in terms of eq.4 yielded narrow relaxation time distributions in all cases and the average diffusion coefficient was calculated using eq.5. The q-dependence of D was found to be weak even for large aggregates when the q-

dependence of I_r/KC was strong, which shows that the aggregates are relatively rigid. For β-lg aggregates it was found that that the rigidity of the aggregates increased with increasing ionic strength [39], which corresponded to increasing degree of branching [42].

R_{hz} was calculated from the average diffusion coefficient extrapolated to q=0 using eq.5 and the ratio R_{gz}/R_{hz} is shown as a function of M_w in figure 8. For non-draining particles this ratio depends on the structure and the size distribution of the particles, but for self similar particles these parameters are independent of the molar mass. We found a weak decrease of the ratio with increasing molar mass of the aggregates tending to 0.9±0.1 for large aggregates. A similar ratio was reported earlier for β-lg aggregates [38].

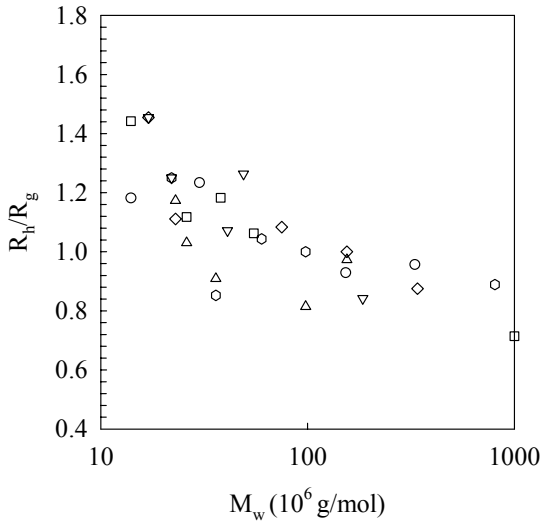

Fig.8 Dependence of the ratio $R_{h\alpha}/R_{ga}$ on the molar mass for myosin aggregates obtained at different heating temperatures, concentrations and pH.

4. DISCUSSION & CONCLUSIONS

It appears that it is very difficult to isolate individual cod myosin. This was already observed half a century ago by Connell [17]. He managed nevertheless to isolate individual myosin using freshly killed cod (pre rigor mortis) using a more rapid method, but probably at the cost of lower purity.

Highly purified myosin from post rigor mortis cod formed small oligomers in dilute aqueous solutions containing 0.5M KCl at pH 6-8 even at low temperatures. The oligomers showed a relatively small variation of R_g and R_h compared to the variation of M_w. This is compatible with the proposition that star-like aggregates are formed by association of the myosin heads based on electron microscopy [5,16,23-25], because for star polymers the radius varies only weakly with the association number (N_{ag}) [37].

Heating the oligomers led in first instance to weak increase of the association number of the aggregates together with a decrease of the both the radius of the gyration and the hydrodynamic radius. This apparently contradictory effect can be explained by the temperature induced helix-coil transition that renders the myosin tails more flexible thus reducing the radius.

Prolonged heating led to further aggregation and finally to precipitation or gelation. It is possible that this second step of the aggregation process is caused by interaction between myosin tails of different oligomers leading to irreversible bond formation between oligomers. Cooling led to a further increase of the size of the aggregates, but this increase was found to be reversible. We may speculate that the bonds formed during cooling involve hydrogen bonds. Another possibility is that coiled-coil structures are reformed after cooling between tails from different oligomers as suggested by Sasaki et al [26]. We note, however, that at higher myosin concentrations large scale aggregation and gelation was observed even at 4°C. This means that the helix-coil transition is not a necessary step for this process.

The outcome of the second step of the aggregation process was the formation of self-similar aggregates similar to those observed by heat induced aggregation of globular proteins. At low protein concentration the growth of the aggregates stagnated at a value that increased with increasing protein concentration. Above a sufficiently high concentration the aggregation process led to flocculation or gelation. Similar observations

were reported for heat induced aggregation of globular proteins[27]. For the latter systems it was found that at a given protein concentration larger aggregates are formed if the electrostatic repulsion is lower [39,40]. For myosin we also found larger aggregates when decreasing pH towards the iso-electric point (pI=5.4), i.e. when reducing electrostatic repulsion.

For globular proteins it was found that the structure of the gels is highly sensitive to electrostatic interactions even though the structure of the aggregates is similar. When the electrostatic repulsion between the proteins was weak, because the pH was close to pI or salt was added, highly heterogeneous turbid gels were observed, while in the opposite case the gels were transparent and homogeneous [27,43]. For the myosin solutions studied here the salt concentration is relatively high so that turbid heterogeneous gels are formed. Such large heterogeneity cannot be explained by simple cross-linking of space filling fractal aggregates and suggests that strong concentration fluctuations or even micro phase separation of the aggregates occurred in more concentrated solutions, while gelation inhibits macroscopic phase separation. Of course, these considerations are speculative and further studies are needed to resolve this issue. Unfortunately, cod myosin solutions are not stable at higher concentrations at low temperatures so that controlled studies of the heat induced gelation process are not possible.

Summary

Highly purified cod myosin was isolated resulting in relatively dilute solutions of oligomers containing around 10 myosin molecules. In addition, large aggregates were formed the extent of which could be reduced by avoiding myosin precipitation steps. Heating led initially to a rapid increase of the association number, but the radius of the aggregates decreased, probably due to the helix-coil transition of myosin tails. At longer times relatively slow aggregation of the oligomers occurred at a rate that increased with increasing myosin concentration (0.4-3g/L), increasing temperature (30-70°C) and decreasing pH (8-6). Cooling extensively heated solutions led to further aggregation, which was, however, reversible upon reheating.

The structure of the aggregates was found to be self similar characterized by a fractal dimension of about 2.2, independent of the concentration, temperature and pH in the range studied here.

5. ACKNOWLEDGEMENTS

The AVS R&D fund of the Ministry of Fisheries in Iceland and The Icelandic Technology Developement Fund are acknowledged for the financial support of this work.

6. REFERENCES

(1) Fukazawa, T., Hashimoto, Y., Yasui, T. *Journal of Food Science* **1961**, *26*, 550-555.

(2) MacFarlane, J. J., Schmidt, G.R., Turner, R.H. *Journal of Food Science* **1977**, *42*, 1603-1605.

(3) Harrington, W. F.;Rodgers, M. E. *Ann. Rev. Biochem.* **1984**, *53*, 35-73.

(4) Elliott, A., Offer, G. *Journal of Molecular Biology* **1978**, *123*, 505-519.

(5) Sharp, A., Offer, G. *Journal of the Science of Food and Agriculture* **1992**, *58*, 63-73.

(6) Takahashi, K. *Journal of Biochemistry* **1978**, *83*, 905-908.

(7) Hermansson, A. M., Harbitz, O., Langton, M. *Journal of the Science of Food and Agriculture* **1986**, *37*, 69.

(8) Tsai, R., Cassens, R.G., Briskey, E.J. *Journal of Food Science* **1972**, *37*, 286-288.

(9) Ishioroshi, M., Samejima, K., Yasui, T. *Journal of Food Science* **1979**, *44*, 1280-1284.

(10) Ishioroshi, M., Samejima, K., Yasui, T. *Journal of Food Science* **1981**, *47*, 114-120.

(11) Samejima, K., Ishioroshi, M., Yasui, T. *Journal of Food Science* **1981**, *46*, 1412-1418.

(12) Morita, J. I., Yasui, T. *Agricultural and Biological Chemistry* **1991**, *55*, 1597-1599.

(13) Fukushima, H., Satoh, Y., Yoon, S.H., Togashi, M., Nakaya, M., Watabe, S. *Journal of Agricultural and Food Chemistry* **2005**, *53*, 9193-9198.

(14) Gill, T. A.;Chan, J. K.;Phonchareon, K. F.;Paulson, A. T. *Food Research International* **1992**, *25*, 333-341.

(15) Kouchi, S., Kondo, S., Ooi, K., Ichikawa, H., Dobashi, T. *Biopolymers* **2003**, *69*, 498-507.

(16) Tazawa, T., Kato, S., Katoh, T., Konno, K. *Journal of Agricultural and Food Chemistry* **2002**, *50*, 196-202.

(17) Connell, J. J. *Biochemical Journal* **1960**, *75*, 530-538.

(18) Connell, J. J. *Biochemical Journal* **1961**, *80*, 503-509.

(19) Davies, J. R., Bardsley, R.G., Ledward, D.A., Poulter, R.G. *Journal of the Science of Food and Agriculture* **1988**, *45*, 61-68.

(20) Johnston, I. A., Walesby, N.J., Davidson, W., Goldspink, G. *Nature* **1975**, *254*, 74-75.

(21) Davies, J. R., Ledward, D.A., Bardsley, R.G., Poulter, R.G. *International Journal of Food Science and Technology* **1994**, *29*, 287-301.

(22) Ogawa, M., Ehara, T., Tamiya, T., Tsuchiya, T. *Comparative Biochemistry and Physiology B-Biochemistry & Molecular Biology* **1993**, *106B*, 517-521.

(23) Walker, M., Trinick, J. *Journal of Molecular Biology* **1986**, *192*, 661-667.

(24) Yamamoto, K. *Journal of Biochemistry* **1990**, *108*, 896-898.

(25) Margossian, S. S., Slayter H.S. *Journal of Muscle Research and Cell Motility* **1987**, *8*, 437-447.

(26) Sasaki, T., Yuan, C.H., Konno, K. *Journal of Food Science* **2006**, *71*, C75-C80.

(27) Nicolai, T. In *Food Colloids. Interactions, Microstructure and Processing*; Dickenson, E.; Leser, M., Eds.; The Royal Society of Chemistry: Cambridge, 2007; pp 35-56.

(28) Kristinsson, H. G. *Journal of Food Biochemistry* **2001**, *25*, 249-256.

(29) Martone, C. B., Busconi, L., Folco, E.J., Trucco, R.E., Sanchez, J.J. *Journal of Food Science* **1986**, *51*, 1554-1555.

(30) Woods, E. F., Himmelfarb, S., Harrington, W. F. *The Journal of Biological Chemistry* **1963**, *238*, 2374-2385.

(31) Brown, W. *Light scattering: principles and developement.*; Clarendon Press: Oxford, 1996.

(32) Higgins, J. S.;Benoit, K. C. *Polymers and neutron scattering*; Clarendon Press: Oxford, 1994.

(33) Berne, B., Pecora, R. *Dynamic Light Scattering*; Wiley: New York, 1976.

(34) Stepanek, P. In *Dynamic Light Scattering*; Brown, W., Ed.; Oxford University Press: Oxford, 1993.

(35) Provencher, S. W. *Computer Physics Communications* **1982**, *27*, 229-242.

(36) Herbert, T. J.;Carlson, F. D. *Biopolymers* **1971**, *10*, 2231-2252.

(37) Daoud, M.;Cotton, J.-P. *J. Phys. France* **1982**, *43*, 531.

(38) Gimel, J. C.;Durand, D.;Nicolai, T. *Macromolecules* **1994**, *27*, 583-589.

(39) Baussay, K.;Le Bon, C.;Nicolai, T.;Durand, D.;Busnel, J. *International Journal of Biological Macromolecules* **2004**, *34*, 21-28.

(40) Weijers, M.;Nicolai, T.;Visschers, R. W. *Macromolecules* **2002**, *35*, 4753-4762.

(41) Hagiwara, T.;Kumagai, H.;Nakamura, K. *Biosci. Biotech. Biochem.* **1996**, *60*, 1757-1763.

(42) Pouzot, M.;Nicolai, T.;Visschers, R. W.;Weijers, M. *Food Hydrocolloids* **2005**, *19*, 231-238.

(43) Clark, A. H. In *Functionnal properties of food macromolecules, 2nd edition*; Hill, S. E.; Ledward, D. A.; Mitchell, J. R., Eds.; Aspen Publishers: Gaithersburg, 1998; pp 77-142.

Appendix 1- Earlier myosin and muscle studies

Introduction

Muscle cells and muscle fibers are highly organized entities, a fact which has allowed them to be investigated using x-ray and electron microscopy[1]. Voluntary muscles are composed of many long fibers. Each fiber has repeating units, called sarcomers, or muscle cells. The fiber is also divided longitudinally into many smaller myofibrils - While the diameter of a muscle fiber might be of the order of 0.05-0.1 mm, the myofibril has a diameter of about 1 μm.

It is customary to classify the protein content of muscles into 3 classes of proteins, according to their solubility- stromal proteins (non-water soluble), sarcoplasmic proteins (soluble in water) and myofibrillar proteins (soluble in water of high salt concentration).

The main stromal protein is the main component of the lamina, or the membrane encapsulating the muscle fiber, that is, collagen 4. Other stromal proteins are reticulin and elastin. Sarcoplasmic proteins are mainly enzymes- haemoglobin, myoglobin and other membrane associated proteins.

The main proteins composing the myofibril are myosin and actin, which are arranged into the so called thick filaments and thin filaments, respectively. Each thick filament contains between 200 and 400 myosin molecules, while the thin filament is a double helix of strands of actin molecules, together with other auxiliary proteins.

The repeating sarcomer unit can be seen in picture 1. The sarcomer is demarcated by 2 Z discs, one on each side. The main component of the discs is α-actinin (100kD).

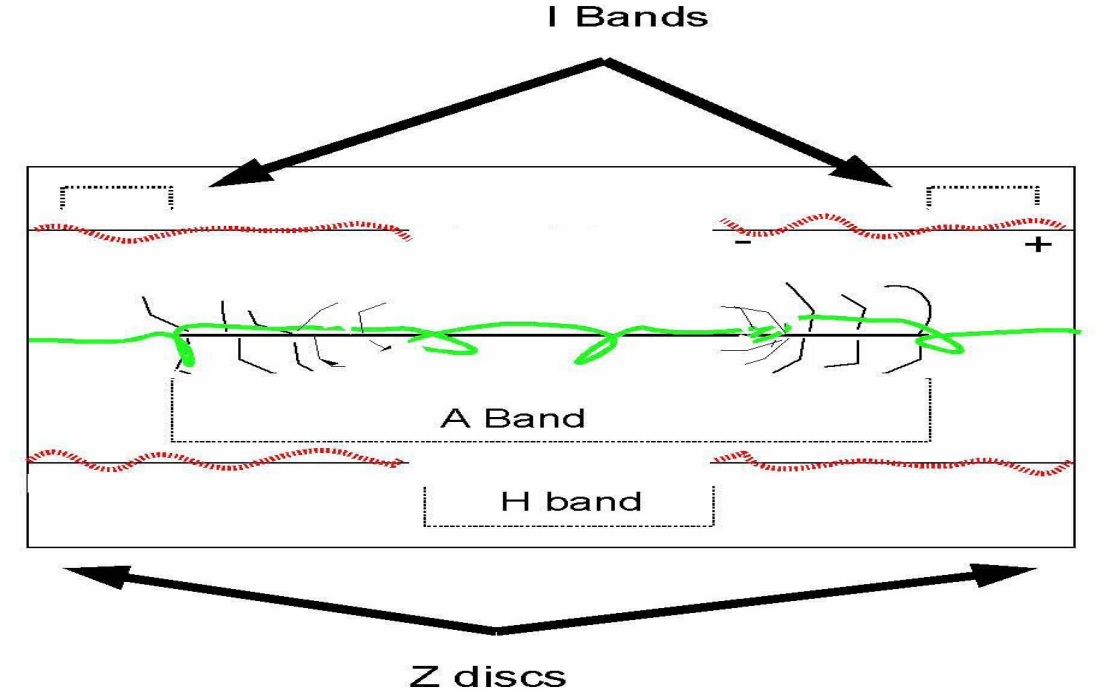

Picture 1 - the sarcomer.

The thick and thin filaments are arranged parallel to each other, with the ends of the actin thin filament attached to Z discs being called the + ends due to their acidic content, while actin filament's end near the middle of the sarcomer is called the – end. The + and – ends are shown for the upper right filament. The myosin molecules change their orientation about the midpoint of the sarcomer. The thin filaments are drawn in red. 2 other important myofibrillar proteins are shown in picture 1, titin and nebulin. Titin is drawn in green, and spans the entire sarcomer longitudinally. It is thought to regulate the thick filament length, and has a Mw of about 3000kD. Nebulin is thought to regulate in a similar manner the thin filaments (drawn in black alongside the actin double helix). Its Mw is around 600kD.

2 other myofibrillar proteins that will be mentioned here are tropomyosin and troponin. Tropomyosin is a fibrous protein, woven along the thin actin filaments. Each tropomyosin molecule in bound to a troponin complex which has 3 subunits called troponin-I, C and T. During rest this tropomyosin-troponin complex blocks myosin from interacting with actin. When Ca^{2+} concentration is increased in the cytoplasm, one Ca^{2+} ion binds to troponin-C which is ensued by a shift in the troponin complex. This exposes

the myosin binding sites on actin, with which myosin can then interact. One actin-binding site is found on each head of the myosin molecule.

2 structural proteins in the myofibril which are low in total content yet important to thick filament arrangement are the C and M proteins. The C protein restricts the thick filaments to about 200 to 400 myosin molecules; the M protein is thought to be responsible for the 3-D arrangement of the thick filaments.

Table 1 lists the main myofibrillar proteins and their mass percentage in the myofibril[2].

Table 1 - myofibrillar content.

Protein	Relative amount (%)	(No. of sub-units)	MW (kD)
Myosin	43-45	2	222
		1 (LC1)	22
		2 (LC2 or RLC)	19
		1 (LC3)	17
Actin	20-23	1	42
Tropomyosin	5	2	35
Troponin	5	1 (TnT)	37
		1 (TnI)	22
		1 (TnC)	18
Titin	8-10	1	2800
Nebulin	3-5	1	600
M protein	2	1	165
C protein	1-2	1	140
F Protein	<1	1	110
α actinin	1-2	2	100

Myosin

The myosin molecule is composed of 2 heavy chains of molecular weight just over 222 kD, and the 4 light chains (LC) which are wrapped around the so-called neck region of the heavy chains, and are numbered LC1, LC2 and LC3 in order of decreasing Mw. There are 2 identical LC2 light chains, which are also called the regulatory light chains

(or RLC), and have a Mw of around 19kD. LC1 and LC3 are referred to as the essential light chains (ELC), and have a Mw of about 22kD and 17kD, respectively. Since they can be released by alkaline treatment, they're also referred to as A1 and A2 light chains.

Enzymatic digestion of myosin with trypsin cleaves it to the so-called heavy meromyosin and light meromyosin (or HMM and LMM). Further cleavage of the HMM with papain gives the S-1 and S-2 fragments, with S-1 usually referring to the myosin head still associated with both one ELC and one RLC light chains. Picture 2 shows the myosin molecule and its fragments.

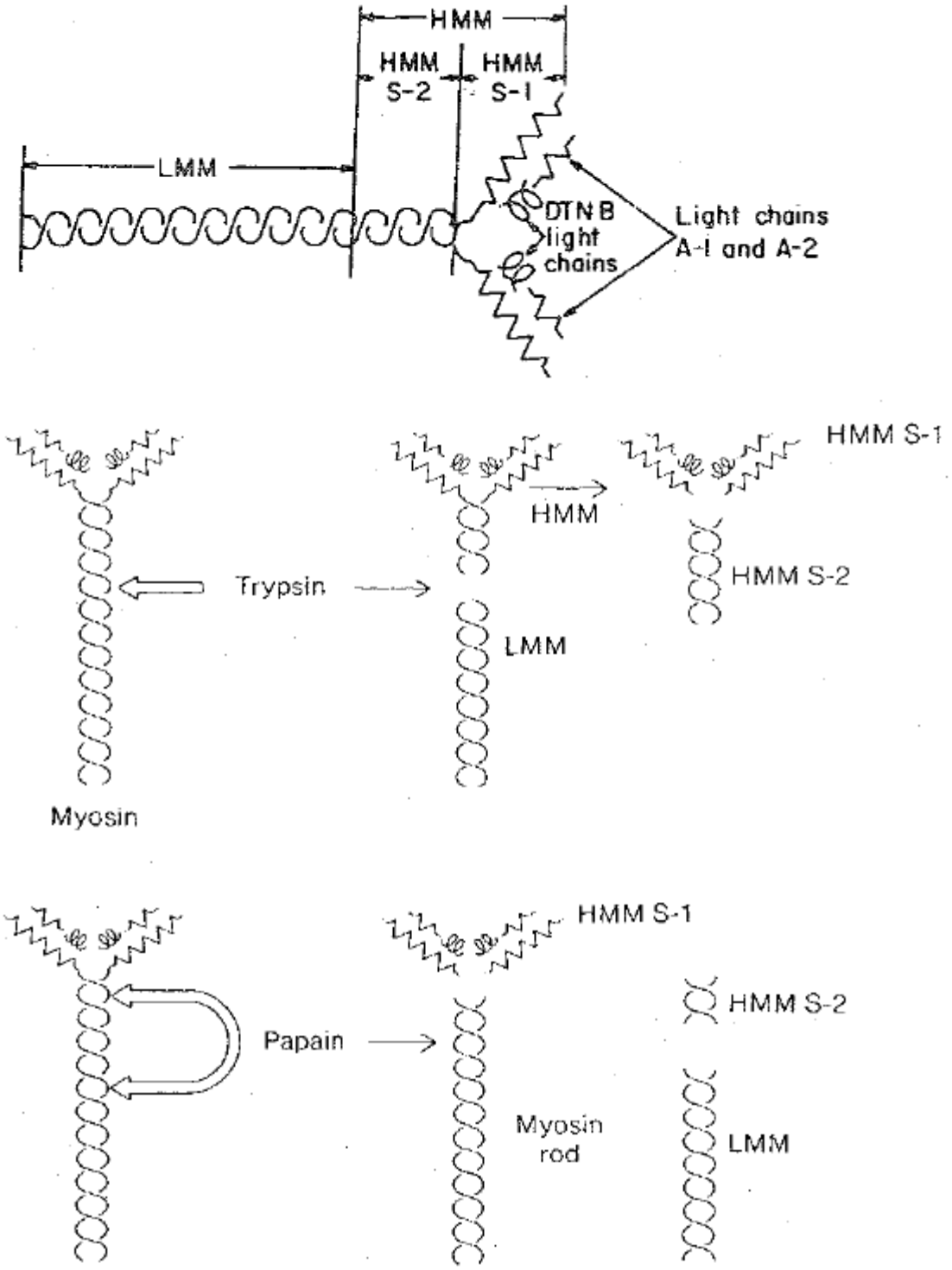

Picture 2- native myosin and the fragments of myosin after different enzymatic treatment.

Size and shape determination of myosin and thick filaments

Determination of the size, shape and flexibility of myosin was first done with electron microscopy. Takahashi[3] reported in 1977 the use of negative staining to visualize the myosin molecule with electron microscopy. He reported the tail region of myosin to be about 140 nm long and 3 nm wide; the heads portions were reported as pear shaped, or an ellipsoid about 21 nm long and 9.5 nm wide near the tail-head junction, while the width reduces to about 5.5 nm further away from the junction. It was also shown that myosin has a very flexible region about 680 nm from the head-tail junction.

Better values, which are accepted today, were obtained (also in 1977) by Elliot and Offer[4]. Myosin molecules were viewed in this study after freeze drying. They reported the tail to be 156 nm long. The heads are reported as pear-shaped and being 18.5 nm long and 6.5 nm wide (in the plane of myosin moiety). The heads width perpendicular to the moiety was reported as 3 nm. Great flexibility was observed in the region about 43 nm from the head-tail junction. This is believed be the region susceptible to proteolytic digestion with trypsin, or in other words the region where scission to HMM and LMM takes place. HMM fragments indeed seem to have a tail region of about 45 to 50 nm, consistent with this data; the length of LMM is, however, less than 110 nm, which suggests that there's some proteolytic damage and the end of LMM is digested. The angles between the tail and the heads were also estimated, and the heads were found to assume a wide range of conformations relative to the tail. The bending of the heads can change the angle between the heads and the tail from about 60° to as much as 250°. The angle between the heads is also varying, so much that the authors claim that it seems the orientation of the two heads is independent of one another.

Quite a few researchers have reported the measurement of native (non-aggregated) purified myosin in aqueous solutions[5-7]. The hydrodynamic values they report are about 25 nm for the myosin dimer and 19 nm for the myosin molecule itself[5,6]. These values are in agreement with the theoretical value proposed by Bloomfield[7]. Wegener[5] used PCS to determine inner modes of motion (bending and rotation) of the myosin molecule; the most interesting results he reported were the maximal bending angle of the myosin heads from the moiety, given to be 42° between each head and the moiety (and, at most, 65° between the heads).

Carlson[6] reports having approximated the molar mass at about 480kD and Rg at 46 nm. Carlson used SLS data to infer a monomer-dimer equilibrium at pH = 7.3, [KCl] = 0.5M and $[PO_4^{3-}]$ = 0.2M. The second virial coefficient A_2 is given as 0.32 lg^{-1}, which is three times higher than the A_2 measured at 0.5M KCl and neutral pH [8] (no phosphate anions). A further increase in pH, however, leads back to a decrease in A_2 to about 0.13 lg^{-1}.

Godfrey and Harrington[9] performed very similar measurements to those of Carlson, but at neutral pH. They could resolve from their data an n-mer which they claimed was larger than a tetramer but smaller than decamer.

Takayama and Fujime[10] have measured myosin under conditions of very low salt concentrations, at pH = 8.3 (5 mM buffer $H_3PO_4/H_2PO_4^-$) and 0.1 mM EDTA. They report the existence of synthetic thick filaments under these conditions (composed of myosin without any auxiliary proteins). They report the measurement of 3 different species of estimated lengths 670, 470 and 300 nm. At Z = 0.134 M, myosin filaments were measured exclusively as 3-filaments (that is, filaments of thickness of 3 myosin molecules) with length of 470 nm. . These filaments are said to have a diameter of 13 nm. Lowering Z to 0.04 M gave, on average, longer and thicker filaments- the average diameter of these filaments increased to 16 nm, and filaments as long as 670 nm were present. The diffusion coefficient D decreased and total light intensity increased with increasing concentration of Mg^{2+}. The authors surmised that the filaments both lengthen and thicken as $[Mg^{2+}]$ is increased from 0 to 3 mM, while the filaments only thicken as $[Mg^{2+}]$ is further increased from 3 to 5 mM.

The diffusion coefficient got larger as total concentration of myosin was lowered, but increased $[Mg^{2+}]$ made this effect less pronounced. Magnesium ions are known to bind to sites in the filament core and stabilize the filament. ATP has the opposite effect on myosin filaments- that is, they break down with increased concentration of ATP. The authors suggest that at 10 mM ATP, the depolymerization to either monomers or dimers is almost complete.

In the onset of the filament breakdown with increased [ATP], the filament is thinning to by about 15%, but remains at constant length; a further increase in ATP concentration led to a shortening of the filaments, as well. At $[Mg^{2+}]$ = 3 mM, the average filament length was 680 nm with no ATP, 470 nm at [ATP] = 2 mM and 300 nm at [ATP] = 5 mM.

Aggregation behaviour of myosin and the thick filaments

Tsunashima and Akugatawa[11] studied the solubility dependency of myosin on myosin concentration, under what they call the "forming conditions" of pH = 7.08, 200 mM KCl and 5 mM phosphate buffer. They found that while the relative amount of soluble myosin decreases with increasing myosin concentration, there is a definite change of this trend around a concentration of 0.2 to 0.4 mg/ml. They concluded that a portion of myosin which is present as a huge aggregate below this concentration breaks down to smaller, soluble aggregates at this concentration. They referred to this transition from an insoluble aggregate to soluble small n-mers a "T-A" transition.

Gelation behaviour and properties of myofibrillar proteins

Investigations of gelation behaviour of purified myosin have been few and far in between, so a mention of more fundamental research of gels made from muscle extracts is at place.

The main component of gels made of muscle extracts, such as surimi, is the myofibrillar proteins[12]. Sufficient salt is added to the solution prior to surimi cooking, which allows for a better solubility of the myofibrillar proteins, which should enhance their ability to form a stable gel.

Many muscle components might have detrimental effect on the gelation properties of the myofibrillar proteins. These might be other proteins, lipids or hydrolysis products of certain enzymes. In the industry, addition of other substances to alter either physical of chemical properties of surimi is quite common. Those substances most used are sorbitol (and other sugars), alcohol and whey proteins. Egg or mammalian proteins may also be added.

Sarcoplasmic proteins, if not totally removed, might affect negatively the gelation properties of muscle extracts. This effect increases if excessive heating and/or foam formation during the surimi cooking lead to denaturation of sarcoplasmic proteins present.

Haemoglobin and myoglobin, which carry a heme group, carry with them ferric ions, which may later oxidise either any lipid "leftovers", as well as certain myofibrillar

proteins. This would affect negatively gel formation. The oxidation of phospholipids or fatty acids "leftovers" usually brings about a strong characteristic fish odour[13], which is also best avoided in food products from an industrial point of view.

Among the enzymes present in the muscle, the 2 most worthy of a mention here are Trimethylamine oxide demethylase and transglutaminase.

Transglutaminase is the name given to a whole family of enzymes. In short, these enzymes catalyze the formation of cross links between proteins by an acyl-transfer. Glutamine and lysine on different parts of a protein, or on different protein molecules, can react to form a bond. The presence of transglutaminase can enhance gelation properties[14].

Trimethylamine oxide (TMAO) is present in all fish as a regulator of osmosis and as an antifreezing agent[15]. Its enzymatic degradation leads to the formation trimethylamine (TMA), a substance of putrid odour which is strongly to spoilage of fish and fish products. While breakdown of TMAO can be catalyzed by a few enzymes (as well as ferric ions, and other proteins high in cysteine content), the most relevant cleavage reaction of TMAO with respect to gel properties is that catalyzed by TMAO demethylase, which forms both TMA and formaldehyde. Formaldehyde is a strong denaturant of proteins, and is known to lead to drier and more brittle gels. Since TMAO demethylase is present in considerable amounts only in salt water fish, and especially in fish of the gadidae family (cods), special preventive steps are required in the post mortem treatment of these fish if the release of formaldehyde is to be prevented. Quick evisceration and boning of the fish can reduce formaldehyde formation, and a longer washing step (leeching) in surimi preparation is thought to help remove TMAO demethylase.

Some myofibrillar proteins have been reported to interfere with surimi preparation. Fractionating extraction can therefore possibly lead to be better gelation properties. The most important myofibrillar proteins reported to negatively affect gel formation are C protein and tropomyosin[16].

Vittayanont *et al*[17] examined gels produced by thermal treatment of chicken breast muscle myosin, and mixed solutions of myosin with β-lactoglobulin. Myosin aggregation patterns, as investigated by turbidity measurements, have a sigmoidal shape, that is, they show that myosin aggregation upon heating starts at a certain temperature, and remains constant or decreases with further heating. Turbidity was reported to increase rapidly up

to about 67°C, and then remained constant. The aggregation rate of myosin was reported to increase with increased myosin concentration, while the temperature at which myosin began to aggregate decreased with increased concentration. Measuring the aggregation during heating of mixed solutions of myosin and β-lactoglobulin, it was found that at low concentration their respective aggregations were separate, and seen as 2 different steps at different temperatures in the turbidity vs. temperature diagram.

The gel point of myosin was decreased with increased concentration. The rheological measurements of myosin supported these results, with higher G' for gels of higher protein concentrations. An interesting feature of myosin's rheograms is that they show two distinct increases in G' when heated. In this study the first increase was measured at about 53°C, and the second at about 73°C. These results are similar to results obtained by other researchers[18]. It was surmised by Smyth *et al*[18] that the tail portion of myosin (LMM) and the head portion (S-1) aggregated first and formed a network at the lower temperature, while S-2 unfolded and added to the network strength at the higher temperature. This is now contested (see discussion below). G' decreased above 75°C, but G' of all myosin and myosin/β-lactoglobulin gels increased upon cooling down, with G' being about 1.4 to 1.7 times larger at room temperature after cooling down from 80°C. This strongly suggests further enhance of gel strength by hydrogen bonds upon cooling. Once last point to note was that the G' of mixed myosin/β-lg gels was lower than that of pure myosin gels (same concentration) until high temperatures were reached in the heating process, at which point the G' of the mixed gels became greater than that of pure myosin gels.

Fish myosin has not received much attention as far as aggregation and gelation studies are concerned. The 2 most interesting papers worth mentioning in this respect are both by Japanese authors. Higuchi *et al*[19] investigated both native and hydrolysed myosin from Walleye Pollack. They mention that while myosin and HMM aggregate upon heating, LMM solutions do not aggregate when heated. It is therefore thought that the head portion of myosin is primarily responsible for myosin aggregation.

Measurements on the α-helix content of native myosin, LMM and HMM were carried out. The α-helix content of LMM is much higher than that of HMM, and decreased much more steeply upon heating. LMM α-helix content decreased from 90% to 21% upon

heating to 60°C, while HMM α-helix content only decreased from 37% to 20% with the same treatment.

As expected, myosin and HMM aggregated upon heating to 60°C, but LMM showed no aggregation. Although LMM solution did not aggregate, adding LMM to myosin solutions during heating led to incorporation of LMM into the aggregates. Adding LMM to HMM solutions while heating led to no such coprecipitaion or coaggregation, and so it is postulated that LMM binds to the tail region of myosin. Another point to note is the release of light chains during heating, as aggregated myosin seems to lose about half of the LC2 and LC3 and almost all of the LC1. The loss of LC2 had been assumed to play a major role in myosin aggregation, through enabling interaction between myosin heads and their subsequent aggregation[20].

The last and very important suggestion of Higuchi et al is that LMM does play a role in myosin aggregation, through network formation of the tails. This is supported by the fact the above mentioned adding of LMM to myosin solutions during heating led not only to their coprecipitaion, but also inhibited the gelation process. Gels obtained in this manner were greatly weakened and broke down some time after formation. This can be rationalized by the fact that if LMM indeed binds to the tail region of native myosin, it might inhibit further interactions between myosin tails which is assumed to be important in formation of a stronger gel network.

Kouchi *et al*[21] investigated gelation of myosin from white croaker. Both light scattering and rheology measurements were made on myosin solutions at neutral pH and 0.6M KCl. Hydrodynamic radii of myosin molecules decreased from around 85 to 65 upon heating, with a steep transition at about 35°C; Rh then remained fairly constant upon further heating, but increased markedly upon cooling, reaching values of about 100 nm with after a steep increase at ~30°C.

Incubating myosin at 30° leads to a definite increase in G'. A subsequent cooling to 0° leads to an even greater increase in G'. This latter increase is reversed by elevating the temperature to 30°C again, but G' increases again when the temperature is elevated beyond 35°C. G' then decreases between 35°C and 45°C, and increases again between 45°C and 60°C. G' invariably increases after the first heating, with the final G' at room temperature or lower weakly dependent on the highest temperature at the heating profile.

The solutions which were heated to 90°C, however, showed a significantly higher G' after cooling than solutions heated to 60-80°C.

From the above results, the following was surmised about the mechanism of myosin aggregation and subsequent gelation: as the temperature is elevated, myosin heavy chains unfold and transform from coiled coil α-helices to random chains. S-S bridges, either intra- or intermolecular, are assumed to form in the head region at around 30-35°C. A subsequent decrease of the temperature may lead to a refold of the α-helices that may interact and enhance the intermolecular network, which would explain the increase in G'. An interaction between tail portions of myosin is also possible through an initial heating to much higher temperatures (>60°C). Formation of disulfide bridges in the tail region is then assumed to take place, which may explain full sol to gel transform upon cooling of these solutions when coupled with the non-covalent interactions which are assumed to commence when the solutions are cooled.

References

(1) Carlson, F.D. In *The Application of Laser Light Scattering to the Study of Biological Motion*; Earnshaw, J.C., Steer, M.W., Ed.; Plenum Publication Corporation: Maratea, 1982.

(2) Stefannson, G., Hultin, H.O .(1994). *Journal of Agricultural and Food Chemistry* **1992**, 42, 2656-2664.

(3) Takahashi, K. *Journal of Biochemistry* **1978**, *83*, 905-908.

(4) Elliott, A., Offer, G. *Journal of Molecular Biology* **1978**, *123*, 505-519.

(5) Wegener, W. *Biopolymer*s **1982**, 21, 1049-1080.

(6) Herbert, T., Carlson, F.D. *Biopolymers* **1971**, 10, 2231-2252.

(7) Garcia de la Torre, J., Bloomfield, V.A. *Biochemistry-US* **1980**, 19, 5118-5123.

(8) Kielley, W.W., Harrington, W.F. *Biochemistry & Biophysics Acta* **1960**, 41, 401.

(9) Godfrey, J.E., Harrington, W.F. *Biochemistry* **1970**, 9, 886-&.

(10) Takayama, S., Fujime, S. *Biophysical Journal* **1995**, 68, 609-618.

(11) Tsunashima Y., Akutagawa, T. *Biopolymers* **2004**, 75**,** 264-277.

(12) Lanier, T.C. In *Surimi And Surimi Seafood;* Park, J.W., Ed.; Marcel Dekker: New York, 2000.

(13) St Angelo, A.J. *Critical Reviews in Food Science* **1996**, 36, 175-224.

(14) Nowsad, A.A.K.M., Katoh, E., Kanoh, S., Niwa, E. *Fisheries Science* **1995**, 61, 1039-1040.

(15) Sotelo, C.S, Rehbein, H. In *Seafood Enzymes;* Haard, N.F., Simpson, B.K., Ed.; Marcel Dekker: New York, 2000.

(16) Sano, T., Noguchi, S.F., Tsuchiya, T., Matsumoto, J.J. *Journal of Food Science* **1989**, *54*, 258-&.

(17) Vittayanont, M., Vega-Warner, V., Steffe, J.F., Smith, D.M. *Journal of Agricultural and Food Chemistry* **2001**, 49, 1587-1594.

(18) Smyth, A.B, Smith, D.M, Vega-Warner, V, O'Neill, E. *Journal of Agricultural and Food Chemistry* **1996**, 44, 1005-1010

(19) Higuchi, T., Ojima, T., Nishita, K. *Fisheries Science* **2002**, 68, 1145-1150.

(20) Sharp, A., Offer, G. *Journal of the Science of Food and Agriculture* **1992**, *58*, 63-73.

(21) Kouchi, S., Kondo, S., Ooi, K., Ichikawa, H., Dobashi, T. *Biopolymers* **2003**, *69*, 498-507.

Appendix 2- Basics of light scattering and its use in characterization of fractal systems

Static Light Scattering (SLS)[1]

The scattering of light from the surface of particles which have different refractive index than the medium in which the light beam travels, is well known[1]. The spectroscopy of scattered light from solutions deals with finding the size, mass and diffusion rate(s) of solute molecules. Scattered light can be thought of as photons scattered in any given time only by solute molecules which happen to be in the scattering volume (designated Vs); the light-scattering particles are moving with different velocities, a thing which gives rise to different interference patterns for the scattered light. The outcome of this is a non-constant intensity of scattered light; we may say this intensity fluctuates, and that the different interference patterns reflect movement of the particles (diffusion). An averaged intensity can be obtained by averaging over a long enough period of time (ideally, that would be $T \to \infty$). We write, then:

$$\langle I \rangle = \frac{1}{T}\int_0^T I(t)dt \qquad (1)$$

The measurement of the averaged intensity over a long period of time is referred to as SLS, or static light scattering. Assuming that the intensity of incident light I_0 is constant, the averaged intensity can be used for analysis of the angle dependency. However, more information can be obtained if we actually know what the intensity of the incident beam is; then we introduce the concept of relative intensity, which refers to the expression $I_r = \frac{\langle I \rangle}{I_0}$, where I_0 is the intensity of incident beam.

In order to relate I_r to some of the characteristic properties of the solute, we'll have to work through some fascinating physics. The quantity $\langle I \rangle$ will henceforth be written as I, except for when we deal with instantaneous intensity in the next section.

We start by considering the intensity of the scattered electric field. When light passes through a medium, the electric field vector causes the molecules to be polarized. The

fluctuating dipoles will radiate energy, in the form of scattered light, in all directions. Total net scattering will be observed if scattering in all directions is not cancelled out, which is indeed the case if there are fluctuations of concentration of the scattering particles on length scales comparable to the inverse of the scattering vector q (discussed below).

Lord Rayleigh (1871) rationalized that the amplitude of the scattered wave should fall off inversely with the distance r. The electric field of the incident light would produce a dipole moment **P** which would be proportional to the polarizability α'. The field of the scattered wave produced by this oscillating dipole would also be proportional to **P**, and hence, to α'. Since α', which in this case is the molar polarizability rather than the molecular polarizability, has the dimensions of volume, and since the relative amplitude of initial and scattered electric field is dimensionless, the ratio should depend on some other variable which has the dimensions m^{-2}. There are in fact many other factors affecting the scattering intensity; they will all be, however, reflected in the characteristic polarizability of the scattering particles. The only parameter not affecting the polarizability is the wave length λ of the incident light, and thus the relative amplitude of scattered and initial electric fields should be inversely proportional to λ^2. The intensity of the light beam is proportional to the square of the amplitude, and thus the relative intensity should follow relation (2):

$$\frac{I}{I_0} \propto \frac{\alpha'^2}{r^2\lambda^4} \qquad (2)$$

Writing the above equation in terms of the wave vector k ($k=2\pi/\lambda$), and returning to the convenient molecular polarizability α ($\alpha = \alpha'/4\pi\varepsilon_0$):

$$\frac{I}{I_0} = \left(\frac{16\pi^4}{r^2\lambda^4}\right)\left[\frac{\alpha}{4\pi\varepsilon_0}\right]^2 \qquad (2b)$$

Equation (2b) is valid for one scattering unit, or in other words the contribution of one scattering unit to the total scattering. Since we are dealing with the case of a solution consisting of solute particles with different dielectric constant than the solvent, we may

treat the polarizability as the difference in the dielectric constant of the solution and the (pure) solvent, divided by the particles' concentration. Then:

$$\alpha = \frac{\varepsilon_0(n_s^2 - n_0^2)}{N_p} = 2\varepsilon_0 n_0\left(\frac{dn_s}{dN_p}\right) = 2\varepsilon_0 n_0 \frac{M}{N_A}\left(\frac{dn_s}{dC}\right) \qquad (3)$$

Where N_p is the number of particles per unit volume. If we introduce now the mass concentration $C=N_pM/N_A$, note that there are N particles making up the total scattering, and then put (3) into (2b), then we get:

$$\frac{I - I_{sol}}{I_0}\frac{r^2}{Vs} = \left(\frac{4\pi^2 n_0^2}{\lambda^4 N_A}\right)\left[\frac{dn_s}{\mathrm{dC}}\right]^2 CMP(\theta) \qquad (4)$$

Where $Vs = N/N_p$ is the scattering volume (the volume encapsulating the N particles involved in the scattering), C is the concentration in mass per unit volume, M is the molar mass and $P(\theta)$ is a dimensionless factor, depending on the phase and polarization of both the incident and the scattered beam. I_{sol} is the scattering from the solvent ($I_r = (I-I_{sol})/I_0$), which should be subtracted from the total scattering, but it is usually negligible compared to the solute scattering. Both sides of equation (4) have the dimensions m^{-1}. In order to relate it to the dimensionless ration $I/I_0=I_r$, we have to find the equipment characteristic ratio r^2/Vs. That can be done if we know the so called Rayleigh ratio for a given scattering solvent, often designated RR. RR has units of m^{-1}. By carrying out a scattering experiment with the given solvent occupying the scattering volume, we know that

$$\frac{I_{tol}}{I_{tol,0}}\frac{r^2}{Vs} = RR_{tol} \qquad (4b)$$

Where the subscript 'tol' stands for toluene, a common refractive index matching solvent. Before we rewrite equation (4) we note that the scattering volume is not necessarily the same for the standard (say, toluene) and the sample's solvent. This is corrected for with $(n_{st}/n_0)^2$, where n_{st} is the standard's refractive index. We can now multiply both sides of (4) with the constant Vs/r^2, writing:

$$\frac{I - I_{sol}}{I_0} = \left(\frac{4\pi^2 n_{st}^{\ 2}}{\lambda^4 N_A} \right) \left[\frac{dn_s}{\mathrm{dC}} \right]^2 \frac{I_{tol}}{I_{tol,0} \cdot RR_{tol}} CMP(\theta) \qquad (4c)$$

For very small particles, the phase of both the incident and scattered beam is the same over the entire surface of the scattering particle. The size of particles referred to here should be small compared to the wave length of the incident beam; we demand that:

$$ka << 1 \qquad (5)$$

for this criterion to be met. The sizes quoted are- a- a characteristic size of the scattering particle, and k- the wave vector, which is equal to $2\pi/\lambda$. We refine (5) by requiring

$$kan << 1, \qquad (5b)$$

where n is the ratio between the refractive index of the scattering particle and the refractive index of the medium ($n=n_p/n_0$).

Adding to condition (5b) the assumption (5b) that scattering from each particle is independent (which is a good approximation for very dilute solutions), it can be concluded that $P(\theta)$ is not angle dependent, and is, indeed, a constant (equal to unity). Scattering which is not angle dependent is referred to as Rayleigh scattering.

The next region of scattering is referred to as the Rayleigh-Gans-Debye (RGD) region. In this region $P(\theta)$ is found to change as a function of the scattering vector q. This function might get very complicated at times. The RGD criteria are:

$$(n-1) << 1 \text{ and } 2ka(n-1) << 1 \qquad (6)$$

If we now define the scattering vector q as

$$q = \frac{4\pi n_0}{\lambda} \sin(\theta/2) \qquad (7)$$

It can now be shown for spherical particles that

$$P(\theta) = \left[\frac{3(\sin(qa) - qa\cos(qa))}{qa^3} \right]^2 = 1 - \left(\frac{(qa)^2}{5} \right) + \ldots \qquad (8)$$

The expansion about $qa = 0$ in equation (8) is valid for small angles (or small values of qa).

In fact, $P(\theta)$ has the same general form for particles of any shape:

$$P(\theta) = 1 - \frac{(qa_g)^2}{3} + \ldots. \qquad (8b)$$

To illustrate this, we can look at $P(\theta)$ for thin, long rod-like particles, of length l^2:

$$P(\theta) = \frac{2}{ql} \int_0^{ql} \frac{\sin u}{u} du - \left[\frac{2\sin(ql/2)}{ql} \right]^2 = 1 - \left(\frac{(ql)^2}{36} \right) + \ldots \qquad (9)$$

Eqn (9) reduces to eqn (8b) when written in terms of a_g. Here, a_g is the **radius of gyration** of the particle (equals to $\sqrt{3/5}a$ for a sphere with radius a, $\sqrt{1/12}l$ for a rod of length l and $\sqrt{1/12}L$ for a Gaussian coil of contour length L).

$a_g = \sqrt{3/5}a$ Sphere (10)

$a_g = \sqrt{1/12}l$ Rod (10b)

$a_g = \sqrt{1/6}L$ Gaussian coil (10c)

It is therefore obvious that plotting I_r against q^2 should yield both the molar mass and the radius of gyration of the scattering particles. This plot requires only one extrapolation (to $\theta = 0$),.

For a non-homogenous solution, we note the molecular polarizability is proportional to $\sum M_i^2$, while c is proportional to $\sum M_i$ .The yielded "average" molar mass is therefore the *weight* average molar mass M_w (rather than the *number* average molar weight M_n). We also note that the measured radius of gyration is the mean square root of R_g, often written R_{gz}.

$$M_w = \frac{\sum N_i M_i^{\,2}}{\sum N_i M_i} \qquad (11)$$

$$M_n = \frac{\sum N_i M_i}{\sum N_i} \qquad (12)$$

The polydispersity, or polydispersity index, is traditionally defined as the ratio of these two measures of average molecular weight, M_w/M_n.

Zimm plot[2, 3, 4]

The aforementioned plot is not taking into account higher expansion terms of eqn. (8) beyond the quadratic term. A more intricate approach was suggested by B.H Zimm back in 1948. Instead of working with the limiting approximations leading to equations (4) and (4c), he worked with the general formula[4]

$$\frac{Kc}{I_r} = \frac{1}{P(\theta)} \frac{\partial \pi / \partial c}{RT} \qquad (13),$$

Where π is the osmotic pressure and $\partial \pi / \partial c$ is the osmotic compressibility. Since

$$\pi = RT\left(\frac{c}{M} + \frac{A_2 c^2}{M} + \frac{A_3 c^3}{M} + \ldots\right) \qquad (14)$$

performing the differentiation and retaining 1 term both in the differentiation and in the Taylor expansion of P(θ), Zimm wrote:

$$\frac{Kc}{I_r} = \frac{1}{M}\left[1 + \frac{\left(q a_g\right)^2}{3}\right] + 2A_2 c \qquad (15)$$

Where

$$K = \left(\frac{4\pi^2 n_{st}^{\ 2}}{\lambda^4 N_A} \right) \left[\frac{dn_s}{\mathrm{d}C} \right]^2 \frac{I_{tol}}{I_{tol,0} \cdot RR_{tol}} \qquad (16)$$

Next, a grid of measurements is set up by measuring solutions of different concentrations at different angles. The function Kc/I_r is plotted against $\sin^2(\theta/2)+bc$, where b is an arbitrary constant, usually chosen to satisfy the relation $bc_{max} \sim 1$. Two kinds of extrapolations are now required: one for each given concentration (at different angles), where the extrapolation is down to $(\theta = 0)$; the other is for a given angle, down to zero concentration. Finally, all the points for zero concentration (at different angles) are extrapolated to zero angle, and the points for zero angle are extrapolated to zero concentration. In the ideal case, the two extrapolations will have the same intersect with the Kc/I_r coordinate, that is the inverse of the weight average molecular mass; the initial slope at $c = 0$ (α_c) should equal $\tan^{-1}\left[\frac{(4\pi n_0 a_g)^2}{3M\lambda^2} \right]$, while the initial slope at $\theta = 0$ (α_θ) is equal to $\tan^{-1}\left[\frac{2A_2}{b} \right]$, where A_2 is the second osmotic virial coefficient. The two dimensional grid set up for the method of double extrapolation is referred to as a **Zimm plot.**

$$\alpha_c = \tan^{-1}\left[\frac{(4\pi n_0 a_g)^2}{3M\lambda^2} \right] \qquad (17)$$

$$\alpha_\theta = \tan^{-1}\left[\frac{2A_2}{b} \right] \qquad (18)$$

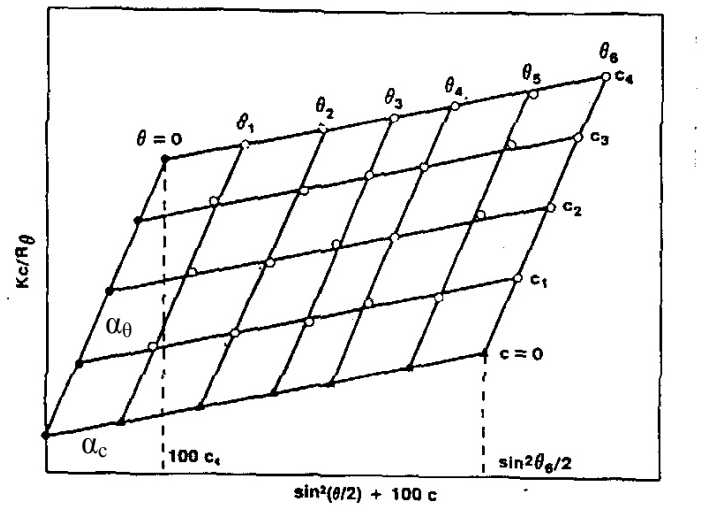

Figure 1- a typical Zimm plot. Image taken from http://www.chem.tu-freiberg.de/~voigt/Studium_Lehre/VORLES_MAT/MOLBAU/folien1.htm

Dynamic Light Scattering (DLS)[3]

While SLS deals with the average scattering of a sample, the domain of dynamic light scattering, or DLS, is the time dependency of the intensity of a scattered beam.

In order to realize the origins of DLS, one should turn to the concept of destructive and constructive interference. The scattering units in the scattering volume are not stationary, but are rather diffusing in a manner that should ideally follow the equations of Brownian motion. The scattered photons, therefore, will be faced with a time dependent interference pattern. This is the origin of the band-width of the scattered beam.

Of course, the signal must fluctuate about its average. Its fluctuation can be characterized by the equations of diffusion, which isn't surprising keeping in mind that the interference pattern is changed as the relative position of scattering particles is changed with diffusion.

If we were to subtract the average value from any given intensity, id est, write:

$$\delta I(t) = I(t) - \langle I \rangle \qquad (17),$$

Then we would get the deviation from the average as a function of time. It is obvious that

$$\int_0^{\infty} \delta I(t)dt = 0 \qquad (18)$$

However, how "fast" does $\delta I(t)$ fluctuate about zero? How long does it "stay" positive before turning negative again, and vice versa? If the motion of particles in the solution is slow, then the interference pattern must also change slowly. If we then plot δ against t we find large regions of negative and positive values. The opposite is true for the case of fast diffusion. If we now define the time lag as $\tau = t_{(1)} - t_{(0)}$, we can see that

$$\frac{1}{T}\int_0^{T\to\infty} \delta I(t)\delta I(t+\tau)dt \geq 0 \qquad (19)$$

In fact, when $\tau = 0, \delta I(t)\delta I(t+\tau) = (\delta I(t))^2 > 0$ and so, $\int_0^{\infty} (\delta I(t))^2$ has a positive value. If the value of $I(t+\tau)$ is highly probable to have the same sign as I(t), then

$$\int_0^{\infty} \delta I(t)\delta I(t+\tau)dt$$

will have a large positive value. This is true for a small time lag- obviously, it should take time for a positive value to change its sign. We recognize in this case that $I(t+\tau)$ and I(t) are highly related. $\frac{1}{T}\int_0^{\infty} \delta I(t)\delta I(t+\tau)dt$ is called the *autocorrelation function* of the property δI. However, as the time lag gets larger, the inner relation between these values is lost; $I(t+\tau)$ is no longer more likely to be of the same sign as I(t). In fact,

$$\lim_{\tau\to\infty} \frac{1}{T}\int_0^{T\to\infty} \delta I(t)\delta I(t+\tau)dt = 0 \qquad (20)$$

So, the autocorrelation function falls from a certain value when $\tau = 0$ to zero when $\tau = \infty$.

We now write:

$$G(\tau) = \frac{1}{T} \int_0^{T\to\infty} \delta I(t)\delta I(t+\tau)dt \qquad (21)$$

$G(\tau)$ holds all the information about the diffusion of scattering particles in the solution. We note that $G(0) = \langle \delta^2 \rangle$ and $G(\tau) \le G(0)$. It can be shown from physical considerations that the time dependent autocorrelation function G fall as an exponential of τ. We can define a characteristic decay time τ_r; now G is an exponential function of τ :

$$G(\tau) = G(0)\exp\left(-2\frac{\tau}{\tau(r)}\right) \qquad (22)$$

We now need only a definition of τ_r to relate $G(\tau)$ to diffusion. It can be shown[3] that

$$\tau_r = (q^2 D)^{-1} \qquad (23),$$

Where q is the scattering vector defined in the previous section and

$$D = \frac{K_b T}{6\pi\eta R_h} \qquad (24),$$

Where K_b is Boltzman's constant, T is the absolute temperature, η is the viscosity of the solution and R_h is the so called hydrodynamic radius. For a sphere, the hydrodynamic radius equals the actual radius; for other shapes, a calculation of the hydrodynamic radius can be very complicated and often impossible to do analytically; table 1 gives the hydrodynamic radius for various shapes[2].

Table 1: values of hydrodynamic radii for different geometries, after Kralchevsky, Danov and Denkov[2].

Shape	**Characteristic dimension(s)**	**Hydrodynamic radius Rh**
Sphere	R	R
Ellipsoid	R, R, pR	$R\left[\frac{3}{4}p\beta+\frac{1}{8}p\delta+\frac{1}{4}\frac{\alpha}{p}\right]^{-1}$ $\delta=\frac{2\left(p^2\beta-1\right)}{p^2-1}$ $\alpha=\frac{p^2\left(1-\beta\right)}{p^2-1}$ $\beta=\frac{\cosh^{-1}p}{p\left(p^2-1\right)^{1/2}}$ For p>1 (prolate ellipsoid) $\beta=\frac{\cos^{-1}p}{p\left(1-p^2\right)^{1/2}}$
Thin rod	L, d (length, diameter)	$\frac{L}{2\ln\left(\frac{2L}{d}\right)}$
Thin disc	R	$\frac{2R}{\pi}$
Gaussian coil	Contour length $= L$ Persistence length $= l_p$	$\frac{L}{2.606\left(\frac{L}{l_p}\right)^{1/2}}$

Use of the heterodyne and homodyne methods in DLS[3]

The aforementioned derivation of the autocorrelation function G is a bit a naïve, in the sense that we don't necessarily use the deviation from a given average as input.

In the so called homodyne method, the autocorrelation function of the intensity of scattered light is measured. In other words, we measure

$$g^{(2)}(\tau) = \frac{1}{\langle I \rangle^2} \frac{1}{T} \int_0^{T\to\infty} I(t)I(t+\tau)dt = \frac{\langle I(t)I(t+\tau)\rangle}{\langle I \rangle^2} = 1 + \exp\left(\frac{-2\tau}{\tau(r)}\right) \qquad (25)$$

The heterodyne method depends on measuring a part of the incident beam which was not scattered. It is therefore much more complicated (measuring such a concentrated beam would damage most detectors). The observable measured in this case is the autocorrelation function of the intensity of the electric field of the scattered light, given by:

$$g^{(1)}(\tau) = \frac{1}{\langle I \rangle} \frac{1}{T} \int_0^{T\to\infty} E^*(t)E(t+\tau)dt = \frac{\langle E(t)^* E(t+\tau)\rangle}{\langle I \rangle} = \exp\left(\frac{-\tau}{\tau(r)}\right) \qquad (26)$$

E, as aforementioned, is the intensity of the electric field of the scattered light, and the asterisk indicates complex conjugation.

Thus, determining $g^{(1)}$ from $g^{(2)}$, and vice versa, is possible. In practice, it can only be done for processes which are statistically independent, where the **Siegert relation** applies:

$$g^{(2)}(\tau) = 1 + \left|g^{(1)}(\tau)\right|^2 \qquad (27)$$

During diffusion, particles in a diluted solution are statistically independent of one another.

Calculating the diffusion coefficient from the measured autocorrelation function

As mentioned above, a particle moving randomly in the solution with a diffusion coefficient D will give rise to a correlation in light intensity which is reflected in the autocorrelation function,cf. Equations (22) and (23). A monodisperse solution should therefore produce a “clean” autocorrelation function g, which will decrease exponentially with the lag time. Fitting an exponential to the given function g should therefore yield D,

which in turn can be used to calculate R_h. If some polydispersity is present, we note that the fitting parameter is the inverse of the relaxation time, or in other words the frequency. Since $\tau_r = (q^2 D)^{-1}$, and $D \propto R_h^{-1}$, it is obvious that the hydrodynamic radius obtained through a single frequency fit ($R_{h,fit}$) is given with:

$$R_{h,fit} = \left(mean(\frac{1}{R_h}) \right)^{-1} \qquad (28)$$

Performing the fitting procedure on g when g is plotted against the frequency should yield, however, the arithmetic mean of R_h. The ratio of the 2 fit R_h values abotained from fitting g against the time domain and the frequency is another measure of the polydispersity of the solution, but it is not equal to the polydispersity index defined earlier (M_w/M_n).

The reader may, by now, be wondering whether more information cannot be exgtracted from the autocorrelation function of a polydisperse solution- after all, each particle, with its own D, is contributing to the autocorrelation function, which will not decrease as a single exponent but rather be a sum of autocorrelation functions with different amplitudes and different exponents (relaxation times). The answer is yes. In 1978, McWhirter and Pike[5] developed a mathematical model which involves an inverse Laplace inversion, which is aimed at giving a complete distribution profile (function) of the solute particles. This inverse Laplace is given with:

$$g^1(\tau) = \int_0^\infty A(\gamma) \exp(-\gamma\tau) d\gamma \qquad (29)$$

A is a distribution function of the particles, telling how much the solution contains of particles with the frequncy γ (γ = q^2D). Again, it is possible to obtain the distribution function by fitting $A(\gamma)$ or alternatively $A(\frac{1}{\gamma})$. Different peaks will correspond to particles with different relaxation times, and the mean relaxation time of a peak in the time domain times the mean frequency of the same peak in the frequency domain is again of a measure of the polydispersity.

Statistical dependence and multiple scattering

When a solution scatters a significant part of the incident LASER beam, it seems to be turbid, and its absorbance becomes significant. The molar weight calculated with equations (4) or (17) must therefore be corrected by the absorbance:

$$M_w = M_a * 10^A \qquad (30)$$

Where Mw is the molar weight, Ma is the apparent molar weight calculated with equations (4) or (17), and A is the absorbance of the solution (for the given path length of the light scattering tube).

Such a turbid solution poses further physical complications, beyond the fact that the total scatter affects the observed molar weight. In a solution where a photon is very likely to be scattered, it is also very likely to be scattered a second time before leaving the scattering volume (or after, if still in the solution's volume); such a scattering, where scattering from one scattering unit is no longer independent of scattering from neighbouring scattering units, is referred to as multiple scattering. Before applying any of the equations presented above for either static or dynamic light scattering, it is necessary to determine the fraction of photons singly scattered, and to determine the 'real' auto-correlation function (made up of the signal due to singly scattered photons). That is done using the so called **cross correlation scattering** technique (or 3D scattering).

A cross correlation measurement involves the use of 2 LASER beams. These beams will be referred to as I_A and I_B. I_A and I_B have the same positioning in the plane of scattering (xy), but are positioned one on top of the other in the direction perpendicular to the plane of scattering (z). The equations relating to cross correlation will be presented without delving into the pertinent physics and without derivation. The autocorrelation function of the light intensity is now given with:

$$g^{(2)}(\tau) = \frac{\langle I_A(t) I_B(t+\tau) \rangle}{\langle I_A \rangle \langle I_B \rangle} = B + \exp\left(\frac{-2\tau}{\tau(r)}\right) \qquad (31)$$

Where B is a measure of how many photons are singly scattered, but also depends on the experimental setup. In the case of no multiple scattering (and a perfect setup), B is ideally equal to 0.25 (not 1).
The fraction F of singly scattered photons is given by[6]:

$$F = \frac{B}{B_0} = \frac{B}{0.25} \qquad (32)$$

Where B is equal to $g^2_{(0)}$-1 of the solution, and B_0 is the $g^2_{(0)}$-1 value of a perfectly transparent solution. B_0 should, as aforementioned, be equal to 0.25, but this should be verified for the specific experimental setup used.
Equation (4c) can now be rewritten for a measurement done with 3D equipment, with the help of equations (30) and (32):

$$\frac{I - I_{sol}}{I_0} = 10^{-A}\left(\frac{4\pi^2 {n_{st}}^2}{\lambda^4 N_A}\right)\left[\frac{dn_s}{\mathrm{dC}}\right]^2 \frac{I_{tol}}{I_{tol,0} \cdot RR_{tol}} CMP(\theta) \frac{0.25}{g^2{}_{(0)} - 1} \qquad (33)$$

Fractal gel model

Before we are prepared to move on to the use of light scattering in the characterization of fractal systems, we should gain some insight into the world of fractals. Seeing as the author's (TB) research deals with protein gels, which are often shown to be associative in nature[7]- and often follow fractal pattern[7, 8]- a discussion of the nature of fractals is in place.

Consider the following equilateral triangles:

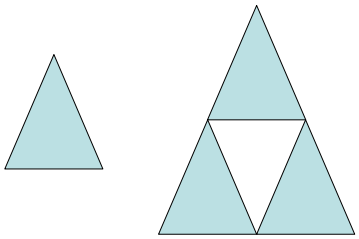

The right triangle can be generated by positioning three triangles similar in size to the left one in a fashion that leaves a "cavity", so to speak, between them; this cavity is equal in area to the left (smaller) triangle. We me say that the smaller triangle has been magnified by 2 in all possible directions. The filled surface of the right triangle of the right triangle is 3 times that of the left triangle. We can carry on augmenting the right triangle and generating larger and larger versions it; this is exactly what is meant with by "fractal nature". We see that the filled surface of the triangle is dependent on the length of the side, but- opposed to a completely filled triangle, the surface A is not proportional to the side length l squared. In fact, it's easy to see that

$$A \propto l^{\frac{\log(3)}{\log(2)}} \cong l^{1.585} \qquad (34)$$

The dependency of surface area on the length, which is a characteristic size of the triangle, is intermediate between that of true "surface" of dimension 2 and that of length (dimension of 1). In general, when one is interested in the dependence of surface, volume or mass (or any other property) on a characteristic size of the system studied, one can define the characteristic dimension of the system (with regard to the property of interest) as:

$$df = \frac{\log(n)}{\log(m)} = \log_{(m)}(n) \qquad (35)$$

Where F is the number of self similar units, and s is the magnification factor. The quantity df is referred to as the **fractal dimension**. When dealing with aggregates of any

kind, the most important fractal dimensions are those referring to the dependency of mass and surface area on the size of the aggregate. The former is simply designated df; the latter is usually designated ds.

Fractal nature of protein gels

It has already been mentioned that protein gels are often associative[7]. This means, basically, that dominant bonds between aggregates which form the gel are non-covalent rather than covalent.

When looking at the fractal nature of these proteins, it is necessary to explain their structure from the microscopic level up. The gels are assumed to be made of aggregates; these aggregates are self-similar. A typical number of protein molecules in an aggregate, is, for instance, 90^9. Somewhat larger aggregates might be referred to as **colloids**. The gel's structure is fractal and consistent with that of the aggregates.

Determining the fractal dimension using light scattering

Now that we know some basics about fractals and fractal structures, let's return for a second to static light scattering. It has already been noted that in the region where $qa_g<1$, the function $P(\theta)$ can be expended as a polynomial function of the scattering vector q and the radius of gyration a_g. In the region where $qa_g>>1$, however, it can be shown for fractal objects that the function $P(\theta)$ is fractal dimension dependent. A few of the references[1, 10, 11] note that in this region the next relation applies:

$$P(\theta) \propto q^{-df} \qquad (36)$$

A plot of $\ln(P(\theta))$ against ln(q) should therefore give a linear relation with –df as its slope.

References

(1) Hunter, R.J. *Foundations of Colloid Science*, Oxford University Press: Oxford, 2001.

(2) Kralchevsky, P.A., Danov, K.D., Denkov, N.D. In *Handbook of Surface and Colloid Chemistry;* Birdi, K.S., ed.; CRC Press: New York, 1997.

(3) Berne, B.J., Pecora, R., *Dynamic Light Scattering*, Dover Publications: New York, 1976.

(4) Brown, W. *Light scattering: principles and developement.*; Clarendon Press: Oxford, 1996.

(5) McWhirter, J.G., Pike, E.R *Journal of Physics A* **1978**, 11, 1729.

(6) Pouzot, M., Nicolai, T., Durand, D., Benyahia, L. *Macromolecules* **2004**, 37, 614-620

(7) Le Bon, C., Nicolai, T., Durand, D. *Macromolecules* **2000**, 32, 1620-1627.

(8) Moret M. A., Miranda, J.G.V., Nogueira Jr. E., Santana, M.C., Zebende, G.F. *Physical Review E* **2005**, 71.

(9) Durand, D., Gimel, J.C., Nicolai, T. *Physica A* **2002**, 304, 253-265.

(10) Aymard, P., Nicolai, T., Durand, D., Clark, A. *Macromolecules* **1999**, 32, 2542-2552.

(11) Amal, R., Raper, J.A., Waite, T.D. *Journal of Colloid Interface Science,* **1954**, 140, 158-168.